IEEE Access
Multidisciplinary | Rapid Review | Open Access Journal

Received February 29, 2020, accepted March 16, 2020, date of publication March 26, 2020, date of current version April 9, 2020.

Digital Object Identifier 10.1109/ACCESS.2020.2983613

Dynamic Coordinated Control Based on Sliding Mode Controller During Mode Switching With ICE Starting for an HEV

AIYUN GAO[1], ZHUMU FU[2,3], AND FAZHAN TAO[2,3]

[1]School of Vehicle and Transportation Engineering, Henan University of Science and Technology, Luoyang 471023, China
[2]School of Information Engineering, Henan University of Science and Technology, Luoyang 471023, China
[3]Henan Key Laboratory of Robot and Intelligent Systems, Henan University of Science and Technology, Luoyang 471023, China

Corresponding author: Zhumu Fu (fzm1974@163.com)

This work was supported in part by the National Natural Science Foundation of China under Grant 61473115, in part by the Scientific and Technological Innovation Leaders in Central Plains under Grant 194200510012, in part by the Science, Technology Innovative Teams in University of Henan Province under Grant 18IRTSTHN011, in part by the Key Scientific Research Projects of Universities in Henan Province under Grant 19A413007 and Grant 20A120008, and in part by the National Thirteen-Five Equipment Pre-Research Foundation of China under Grant 61402100203.

ABSTRACT Due to the friction-induced discontinuity of the clutch torque and ICE on/off, seamless mode transition of hybrid electric vehicles (HEVs) is difficult to achieve, which has a bad influence on the vehicle ride comfort. In the face of system uncontinuity and strong nonlinearity during mode switching with ICE starting, a control strategy of torque dynamic coordination is proposed by means of sliding mode control based on disturbance compensation. Firstly, the steady-state and transient models of parts and working modes are built, which improves modeling accuracy and adaptability to transient driving cycle. Furthermore, the switching process from pure electric driving to hybrid driving is divided into three phases including internal combustion engine (ICE) starting, speed synchronization and torque redistribution. The design of according disturbance observer and sliding mode controller is described in detail. Lastly, compared with other two control strategies, the rationality and validity of the control method designed are testified not only by computer simulations but also experimental tests under the comprehensive driving cycle of local passenger vehicles. The potential of the proposed control strategy in terms of power transfer smoothness and improving riding comfort is illustrated.

INDEX TERMS Hybrid electric vehicle (HEV), coordinated control, sliding mode control, mode switching.

I. INTRODUCTION

It is now widely accepted that the development of hybrid electric vehicles (HEVs) is a promising short term solution to better fuel economy and emissions without compromising vehicle performances [1]–[3]. Instead of having one power source, HEVs have two or more power sources that can act independently or in combination. As a result, HEVs should make transitions between different modes to achieve an optimal power distribution [4], [5]. During the mode switching, particularly the mode switching with the internal combustion engine (ICE) starting, such as from pure electric driving mode to ICE or hybrid driving mode, clutch engagement/disengagement and ICE on/off cause torque disturbance to the drivetrains and increase the vehicle jerk, which is uncomfortable to passengers [6]–[8]. Therefore, it is very important for HEVs control to ensure smooth vehicle operation during the mode transition [9]–[11].

Various mode switching methodologies have been applied to HEVs dynamic coordinated control. These proposed methods include online estimation of the ICE speed [12], [13], model predictive control (MPC) [14], [15], disturbance compensation [16], [17], and so on.

Based on the difference of torque response time between the motor and the ICE, the first method estimates the ICE speed on-line and thus controls motor torque in real time to compensate the ICE torque delay. Tong [18] established average value model of a gasoline engine to achieve real-time estimation of the ICE torque. According to the ICE transient speed, Li *et al.* [19] built ICE torque feedback,

The associate editor coordinating the review of this manuscript and approving it for publication was Huiping Li.

which was applied to HEV dynamic coordinated control successfully. Yan, *et al.* [20] founded the ICE dynamic model based on neural networks in which three parameters including the ICE speed, throttle opening and its change rate were regarded as inputs. These studies all partly improve the ride comfort and reduce the fluctuations of the output torque during mode transition, but there are some problems such as modeling complexity, poor real-time and high requirement for equipments control accuracy during mode transition.

The second approach is realized through strategies of multi-step tests, online rolling optimization of performance indices and feedback correction. Koprubasi *et al.* [21] designed a mode transition controller for a parallel HEV with the switched theory of hybrid dynamical systems to reduce vehicle longitudinal impact. Zhao *et al.* [22] established main parts models and switching models between different modes and then proposed an undisturbed control strategy. These studies proved that MPC can reduce the modeling errors and uncertainties of structure, parameters, and environment. In a word, MPC is known for its simplicity of considering constraints and good robustness and stability. Yet, MPC isn't fit for steady systems and it's difficult to identify system model online.

The third method estimates a disturbance variable of the ICE torque ripple on-line by using a disturbance observer and thus betters the vehicle drivability. Kim, *et al.* [23] developed a model transition control using a disturbance observer for a parallel HEV, where time-dependent parameters in the powertrain model were identified in real time to improve the control system robustness. Kim *et al.* [24] evaluated external disturbance through transfer function and then took into account parameter uncertainties. According to these, a control method of clutch sliding was presented based on interference compensation, hence the ride comfort during mode switching was improved. To a certain extent, these studies all promote control accuracy and enhance the vehicle drivability, but nolinear and uncertainty aren't taken into consideration [25], [26]. It's necessary that this method be combined with other control approach like sliding mode control.

The recent researches indicate that there are larger torque fluctuation and vehicle jerk for mode switching with ICE starting than that without ICE starting. Thus, this paper mainly studies mode switching with ICE starting.

As to mode switching with ICE starting, there are uncontinuity and strong nolinear in HEV due to clutch engagement/disengagement. Sliding mode control has typical adaptability and robustness, so this paper adopts sliding mode control based on disturbance compensation to study the control strategy, which increases system robustness and improves power transfer smoothness in switching process.Then, this paper takes into consideration uncertainty and error of the system model that is regarded as other disturbances. Furthermore, the switching process from pure electric driving to hybrid driving is divided into three phases

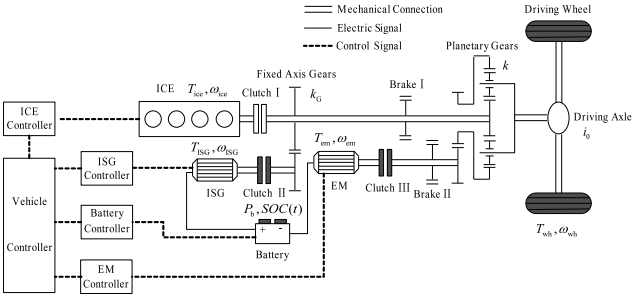

FIGURE 1. Architecture diagram of the HEV.

according to the state of the clutch and ICE and control target, which is beneficial to design more rational control strategy. Lastly, this paper not only establishes the steady-state models of parts and working modes, but also their transient models, which improves modeling precision and adaptability to transient driving cycle such as mode switching.

The remainder of this paper is organized as follows. Section II introduces an architecture of the HEV. Section III then presents the design of steady and transient models for parts and mode switching. A control strategy of torque dynamic coordination is described in Section IV in detail. Control method validation and results analysis are discussed in Section V. Section VI highlights this paper's key conclusions.

II. VEHICLE ARCHITECTURE

The architecture diagram of the HEV is shown in Fig. 1. The ICE is firstly torque coupled by the ISG through fixed axis gears mechanism, whose output is then speed coupled by the electric motor (EM) by way of planetary gears mechanism to finally drive the vehicle via the driving axle. Thus, the vehicle architecture belongs to a hybrid electromechanical coupling scheme which can both realize separate control to two speeds and two torques of power sources. Three clutches and two brakes are added so as to ensure that multi-source of power can work independently or together. Thus, more working modes are achieved. The ICE, ISG, EM and batteries all have respective controller, which is in the control of the vehicle controller.

III. HEV MODELING

A. MAIN PARTS MODELING

1) ICE MODELS

Not only the steady model but also the transient model is built in this paper.

The ICE steady model is established based on the steady-state test data of the ICE. By bench test, the efficiency map of the ICE on the speed-torque plane is obtained and shown in Fig. 2, which can be used to account for the energy management strategy based on ensuring the ICE working in high efficiency region.

The transient models of the ICE are obtained from basic physical and thermodynamic principles.

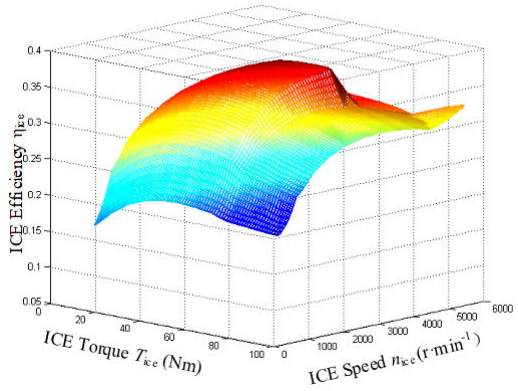

FIGURE 2. ICE steady operating efficiency map.

The crankshaft rotational dynamics is obtained from the Newton's law.

$$T_{\mathrm{ice,e}} = I(\frac{\pi}{30}\dot{n}_{\mathrm{ice}}) = T_{\mathrm{ice,i}} - T_{\mathrm{ice,f}} - T_{\mathrm{ice,l}} \tag{1}$$

where $T_{\mathrm{ice,e}}$ is the effective torque of the ICE, I is the inertia moment of the crankshaft, $T_{\mathrm{ice,i}}$ is the indicated torque of the ICE due to the gas pressure torque, $T_{\mathrm{ice,f}}$ is the friction torque of the ICE, $T_{\mathrm{ice,l}}$ is the load torque of the ICE. It is noted that $T_{\mathrm{ice,i}}$ is the output required for the ICE dynamics, and $T_{\mathrm{ice,f}}$ is subtracted from the instantaneous indicated torque value to produce the brake torque at the shaft. Subsequently, $T_{\mathrm{ice,l}}$, which is the result of external loading imposed on the ICE by the vehicle or the dynamometer, is subtracted from the brake torque and the net value is passed to the ICE dynamics sub-model.

The inertia moment of the crankshaft I is divided into the fixed inertia of the crankshaft (flying wheel) I_{f} and the variable inertia I_{v} due to the crankshaft angle θ, which is expressed as follows.

$$I = I_{\mathrm{f}} + I_{\mathrm{v}}(\theta) \tag{2}$$

The variable inertia I_{v} is the result of the reciprocating and rotating motion of crankshaft mechanism. The Lagrangian equation governing the instantaneous inertia for four cylinders may be written in following form [27].

$$I_{\mathrm{v}}(\theta) = 2m_{\mathrm{r}}R^2(1-\cos(2\theta)) + \frac{m_{\mathrm{r}}R^4}{2L^2}(1-\cos(4\theta)) \tag{3}$$

where m_{r} is the reciprocating mass of crankshaft, R is the crank radius, and L is the connecting rod length.

For in-line ICE, the indicated torque $T_{\mathrm{ice,i}}$ is expressed as below.

$$T_{\mathrm{ice,i}} = \sum_{\mathrm{j}=1}^{n_c} \frac{p_{\mathrm{i,j}}(\theta, n_{\mathrm{ice}}, \phi)\pi D^2 R}{n_{\mathrm{c}}} \cdot \sin(\theta - \alpha_{\mathrm{j}})[1 + \frac{R}{L}\cos(\theta - \alpha_{\mathrm{j}})] \tag{4}$$

where $p_{\mathrm{i,j}}$ is the gas pressure in the j-th cylinder, n_{c} is the number of the cylinders, and α_{j} is the angle phase for the j-th cylinder.

Davis and Lorenz [13] proposed a method of calculating individual cylinder pressure waveforms $p_{\mathrm{i,j}}$ at any n_{ice} and any ϕ as follows.

$$V(\theta) = V_{\mathrm{d}} + \frac{\pi D^2}{4}(R + L - R\cos\theta - \sqrt{L^2 - R^2\sin^2\theta}) \tag{5}$$

$$p_{\mathrm{c}}(\theta) = p_{\mathrm{m}}(\frac{V_{\mathrm{d}} + V_{\mathrm{c}}}{V(\theta)})^e \tag{6}$$

where $V(\theta)$ is the cylinder dynamic volume, V_{d} is the cylinder displaced volume, D is the cylinder bore diameter, $p_{\mathrm{c}}(\theta)$ is the motoring prototype waveform, p_{m} is the manifold pressure, V_{c} is the cylinder clearance volume, and e is the exponent representing the isotropic expansion.

$$p_{\mathrm{i,j}}(\theta, n_{\mathrm{ice}}, \phi) = p_{\mathrm{c}}(\theta)\cdot c_1(n_{\mathrm{ice}}) + \triangle p(\theta)\cdot c_2(n_{\mathrm{ice}}, \phi) + p_0(n_{\mathrm{ice}}) \tag{7}$$

where c_1 is a scaling factor that is a function of n_{ice} and can be founded from experimental motoring data, $\triangle p(\theta)$ is the firing prototype waveform, c_2 is a scaling factor that is a function of n_{ice} and ϕ, $p_0(n_{\mathrm{ice}})$ is the offset pressure.

In a word, firstly, from Eqs. (5-7), $p_{\mathrm{i,j}}$ can be estimated from p_{m} roughly. Then, $T_{\mathrm{ice,i}}$ is got by substituting $p_{\mathrm{i,j}}$ in Eq. (4) and I is acquired from Eqs. (2-3). Lastly, the dynamics model of the ICE is obtained by substituting $p_{\mathrm{i,j}}$ and I in Eq. (1).

2) EM AND ISG MODELS

The EM and ISG are both permanent magnet synchronous motors controlled through direct torque. Because reaction time of the motor is much faster than that of the vehicle and other parts, it's only necessary to establish steady model of the motor.

Similar to the ICE, the efficiency maps of the motor are achieved by fitting. The motor characteristic is based on the efficiency data obtained from experiments. Fig. 3 shows the efficiency map of the motor on the speed-torque plane.

Seen from Fig. 3, the EM efficiency is poor under low torque and low speed, yet the ISG efficiency is higher. Thus, the ISG can work alone as a substitute for the ICE or EM when the velocity or demanding torque of the vehicle is small. Accordingly, powertrain efficiency is raised.

3) BATTERY MODEL

Li-ion battery is selected as energy storage mechanism. Its model is simplified as the circuit system in which an ideal voltage source is in series with an equivalent internal resistance. In charging or discharging condition, the relationship and value of the equivalent internal resistance R_{b} and the open circuit voltage U_{oc} can be interpolated by the constructed table.

The battery efficiency is greatly relative to its remaining electricity, which is represented by state of change (SOC). The tests show that the battery efficiency is approximately 90% if SOC locates between 0.35 and 0.75. Because the battery in HEVs is not designed to be charged from the grid, the energy in the battery should be supplemented to avoid

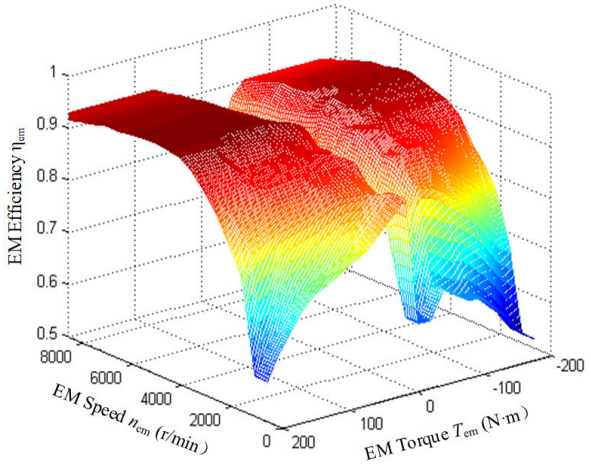

(a) EM

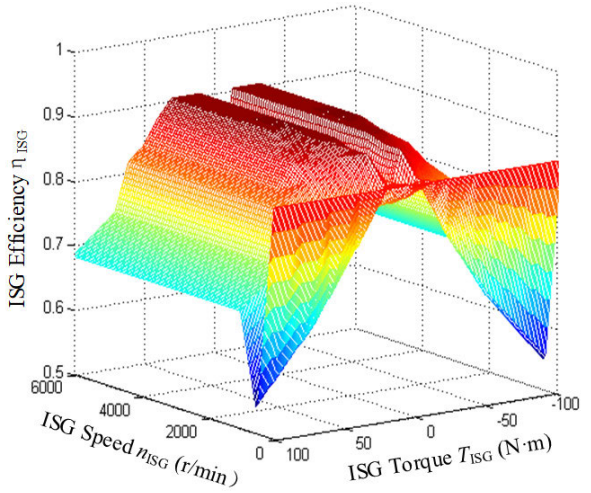

(b) ISG

FIGURE 3. The motor steady operating efficiency map.

the damage [28], [29]. Thus the control strategy should try to maintain *SOC* in its optimal range [30].

The battery *SOC* can be predicted by the following equation.

$$SOC = SOC_0 - \frac{\int_{T_0}^{T} i_b dt}{C_b} = SOC_0 - \frac{\int_{T_0}^{T} U_{oc} - (U_{oc}^2 - 4R_bP_b)^{1/2} dt}{2R_bC_b} \quad (8)$$

where SOC_0 is the initial value of the battery *SOC*, T_0 is the initial value of the time, i_b is the charging or discharging current, C_b is the total capacity, and P_b is the effective power of the battery.

B. MODELING OF WORKING MODES

By using of a hybrid electromechanical coupling mechanism shown in Fig. 1, the HEV can accomplish twelve working modes. According to working modes division and power flow analysis, bond graph models in every operating mode are built under Matlab / Simulink / BondHEV, which provide

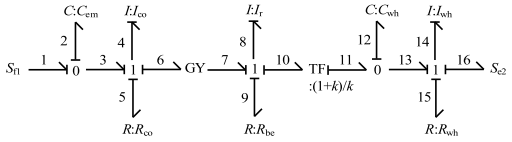

FIGURE 4. The bond graph model in pure electric driving 1.

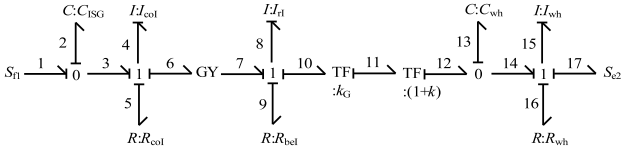

FIGURE 5. The bond graph model in pure electric driving 2.

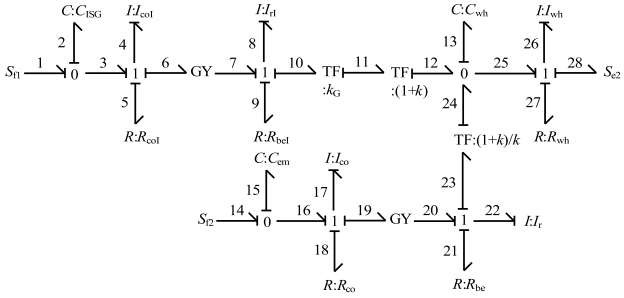

FIGURE 6. The bond graph model in pure electric driving 3.

simulation models for the HEV dynamic coordinated control. For this paper mainly studies mode switching with ICE starting, bond graph models in pure electric driving, ICE driving and hybrid driving are just given.

1) MODELING IN PURE ELECTRIC DRIVING

According to working mode division, there are three modes of pure electric driving owing to three power sources.

The EM works alone, yet ISG and the ICE don't operate in pure electric driving 1 whose bond graph model is shown in Fig. 4.

In Fig. 4, S_{f1} is input, C_{em} is the flexibility of EM rotating shaft, I_{co} is the inductance of exciting coil and armature coil in EM, R_{co} is resistance of exciting coil and armature coil in EM, I_r is the inertia moment of EM rotor, R_{be} is the damping loss of EM bearings, k is the characteristic parameter of planetary gears mechanism, subscript wh is the wheel, S_{e2} is output.

The ISG works alone, yet EM and the ICE don't operate in pure electric driving 2 whose bond graph model is shown in Fig. 5.

In Fig. 5, C_{ISG} is the flexibility of ISG rotating shaft, I_{coI} is the inductance of exciting coil and armature coil in ISG, R_{coI} is resistance of exciting coil and armature coil in EM, I_{rI} is the inertia moment of EM rotor, R_{beI} is the damping loss of EM bearings, K_G is the ratio of fixed axis gears mechanism.

The EM and ISG work together, yet the ICE doesn't operate in pure electric driving 3 whose bond graph model is shown in Fig. 6.

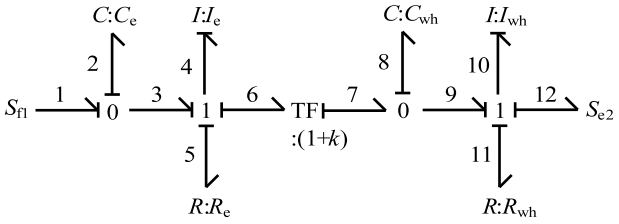

FIGURE 7. The bond graph model in ICE driving.

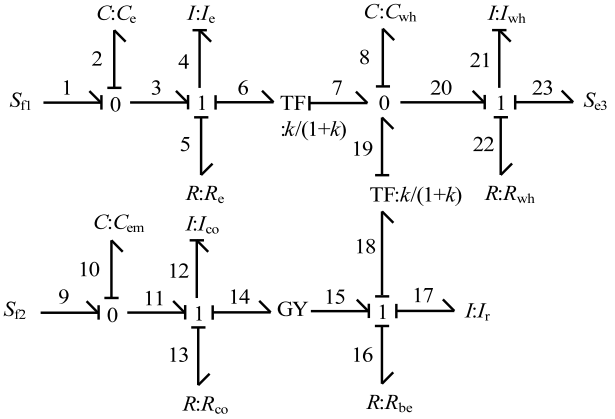

FIGURE 8. The bond graph model in hybrid driving 1.

2) MODELING IN ICE DRIVING

The ICE works alone, yet the EM and ISG don't operate in ICE driving whose bond graph model is shown in Fig. 7.

In Fig. 7, C_e is the flexibility of ICE output shaft, I_e is the inertia moment of ICE, R_e is the damping of ICE.

3) MODELING IN HYBRID DRIVING

According to working mode division, there are three modes of hybrid driving owing to three power sources.

The ICE and EM work together, yet ISG doesn't operate in hybrid driving 1 whose bond graph model is shown in Fig. 8.

The ICE and ISG work together, yet EM doesn't operate in hybrid driving 2 whose bond graph model is shown in Fig. 9.

The ICE, EM and ISG work together in hybrid driving 3 whose bond graph model is shown in Fig. 10.

IV. DESIGN OF DYNAMIC COORDINATED CONTROL STRATEGY

As to mode switching with ICE starting, there are uncontinuity and strong nolinear in HEV due to clutch engagement/disengagement. Sliding mode control has typical adaptability and robustness [31], so this paper adopts sliding mode control based on disturbance compensation to study the control strategy.

The torque response time of the motor is much faster than that of the ICE, so switching between two motors has a small influence on ride comfort [32]. Therefore, this paper doesn't discuss switching between pure electric driving modes, that is to say, EM and ISG are regarded as a motor below. Take the mode switching from pure electric driving to hybrid driving for an example, the design process is as follows.

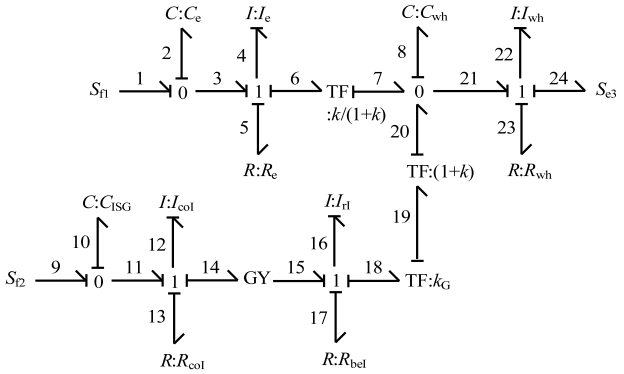

FIGURE 9. The bond graph model in hybrid driving 2.

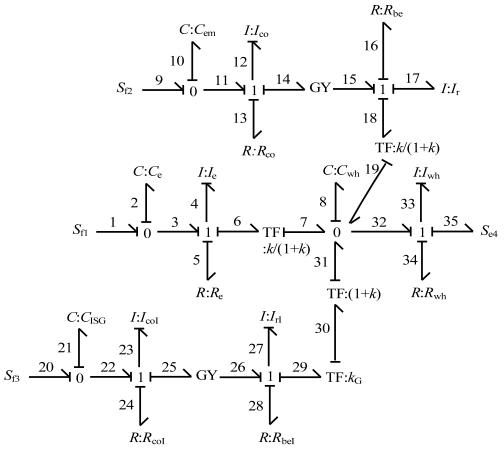

FIGURE 10. The bond graph model in hybrid driving 3.

The flow chart of the dynamic coordinated control is shown in Fig. 11. According to the driver intention and driving cycle signals, the energy distribution control strategy is responsible for optimal energy distribution among multiple power sources under the steady-state driving cycle (such as in some working mode). Yet, the dynamic coordinated control strategy is used to ensure power transfer smoothness under the transient driving cycle (such as during different mode switching). Meanwhile, the energy distribution control strategy provides the target torque in every mode and mode switching condition for the dynamic coordinated control strategy. The energy distribution control strategy isn't discussed in this paper any more and seen in [33] for details. In the following, the design of the dynamic coordinated control strategy will be described in detail.

A. MODE SWITCHING PRINCIPLE

Mode switching principle is shown in Fig. 12.

In Fig. 12, ψ is the switching signal, $i = 1, 2, 3$ is the phase symbol of ICE starting, speed synchronization and torque redistribution respectively, SMC is the sliding mode controller, DOB is the disturbance observer, d is the other disturbance that isn't observed by the disturbance observer, such as uncontinuity and error of the system model that aren't usually taken into account in present researches.

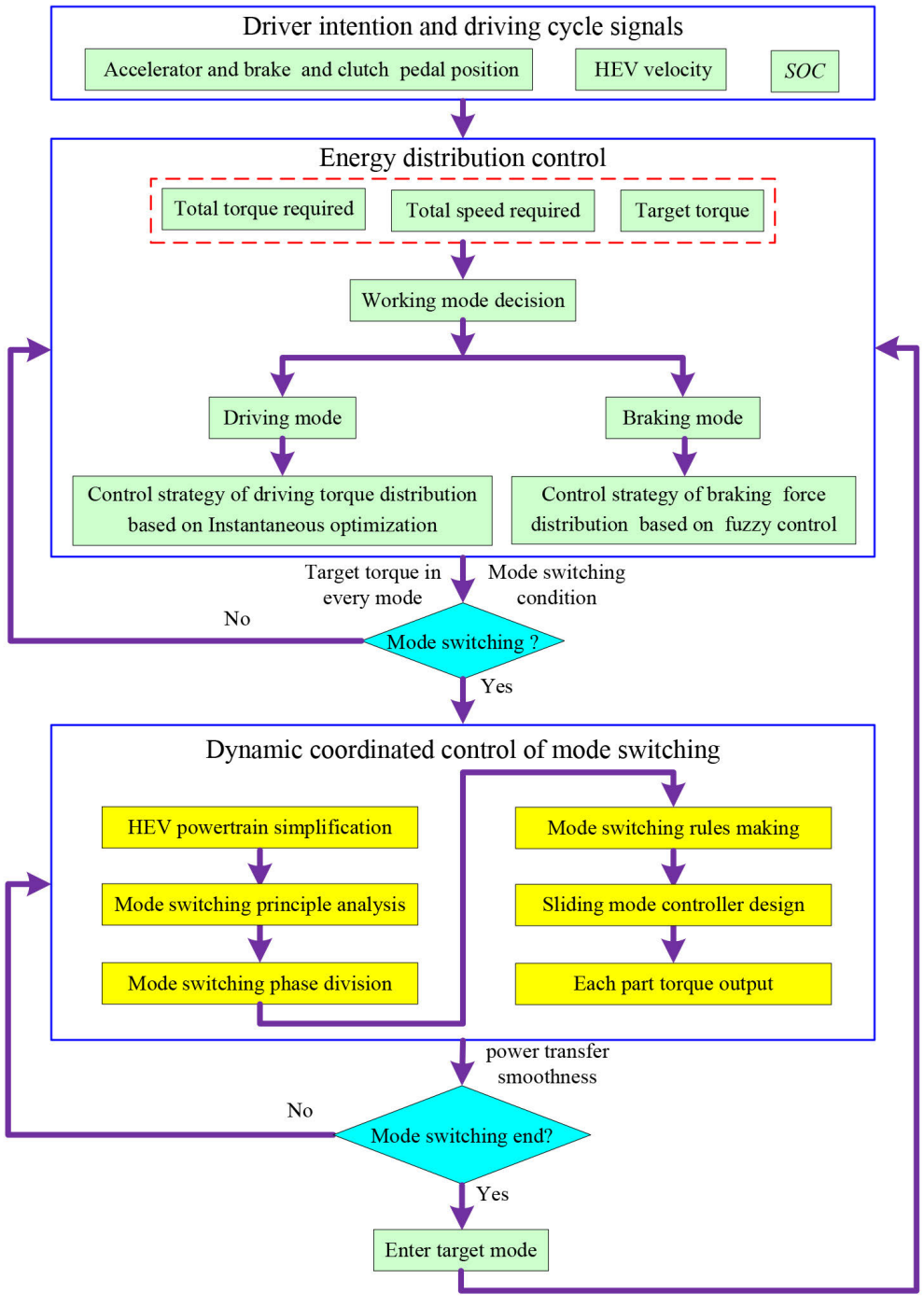

FIGURE 11. Flow chart of the dynamic coordinated control.

Seen from Fig. 12, according to the state of the clutch and ICE and control target, the switching process from pure electric driving to hybrid driving is divided into three phases that include ICE starting, speed synchronization and torque redistribution. Firstly, the system current phase is judged by switching rules and parts real-time torque/speed. Secondly, the according DOB and SMC of each phase are designed. The system input is adjusted by DOB estimate, and the sum of DOB estimate and the other disturbances (d) is compensated by SMC to achieve smooth switching. Lastly, main parts including the ICE, motor and clutch are controlled by according controller so as to accomplish mode switching.

B. MODE SWITCHING RULES

The brake I in Fig. 1 is used to accomplish more working modes for the energy distribution control, whose working state is described in detail in Reference [33]. Because this paper mainly discusses the mode switching, the brake I is

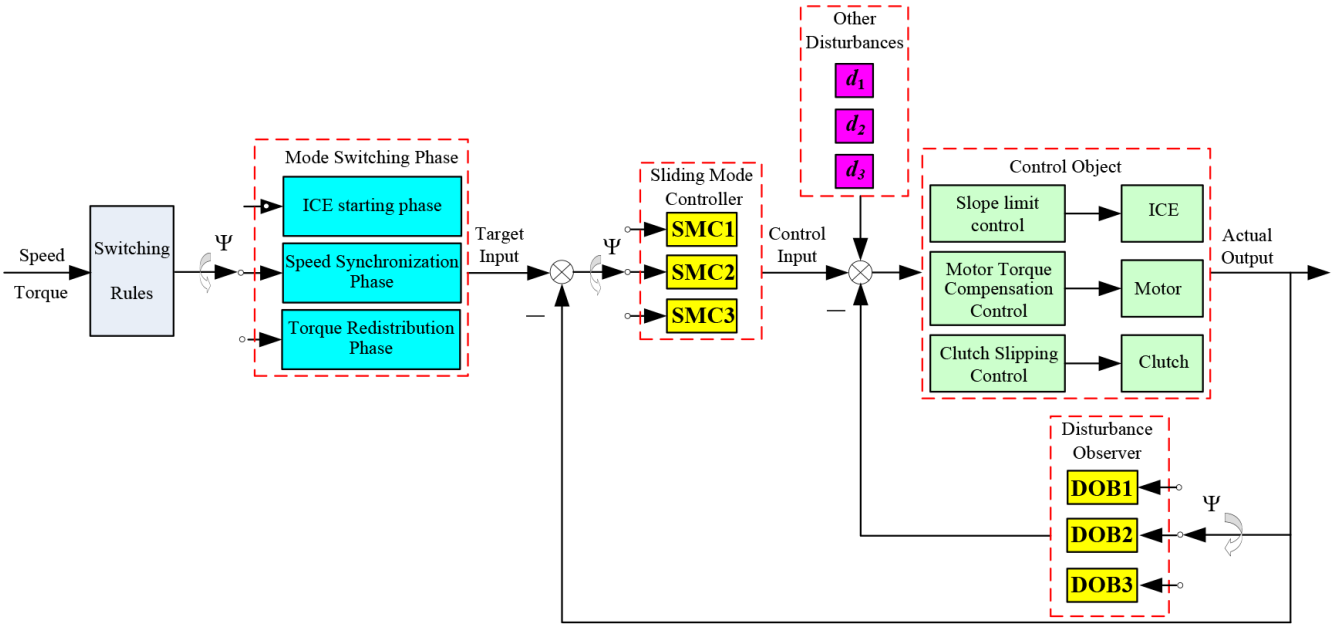

FIGURE 12. Mode switching principle.

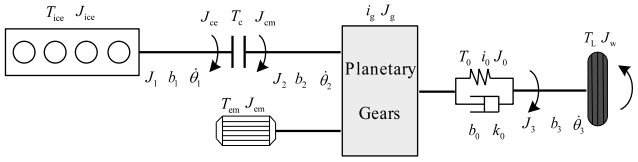

FIGURE 13. Simplified structure of HEV powertrain.

supposed to be always released. Moreover, this paper doesn't discuss switching between pure electric driving modes, that is to say, EM and ISG are regarded as a motor. In this way, simplified structure of HEV powertrain in Fig. 1 is shown in Fig. 13 to take into account elastic constant and damping coefficient of each part.

In Fig. 13, J_1, J_2 and J_3 are the effective inertia moment of the ICE side, EM side and the wheel side respectively, b_1, b_2 and b_3 are their damping coefficient respectively, $\dot{\theta}_1$, $\dot{\theta}_2$ and $\dot{\theta}_3$ are their angular speed respectively, J_{ice}, J_{em}, J_{w}, J_{g} and J_0 are the inertia moment of the ICE, EM, wheel, planetary gears and driving axle severally, J_{ce} and J_{cm} are the clutch inertia moment of the driving disc and driven plate, T_{ice}, T_{em}, T_{c}, T_0 and T_{L} are the torque of the ICE, EM, clutch, and load severally, b_0 and k_0 are the damping and elastic coefficient of the driving axle, i_{g} and i_0 are the gear ratios of the planetary gears and main reducing gear.

Every phase state, control target and switching rules are shown in Table 1 during mode switching, which develops the basis for design of the sliding mode controller.

C. DESIGN AND STABILIZATION PROOF OF THE SLIDING MODE CONTROLLER

1) ICE STARTING PHASE

In this phase, ICE angular speed goes through from 0 to $\dot{\theta}_{\text{ice,idle}}$. ICE acts as the system load, that is, $\dot{\theta}_1$ isn't equal to $\dot{\theta}_2$. Here HEV dynamics equations are expressed as follows.

$$\begin{cases} J_1\ddot{\theta}_1 + b_1\dot{\theta}_1 = T_{\text{c}} - T_{\text{ice,sta}} + f_1 \\ J_2\ddot{\theta}_2 + b_2\dot{\theta}_2 = T_{\text{em}}/i_{\text{g}} - T_0/i_{\text{g}}i_0 - T_{\text{c}} + f_2 \\ J_3\ddot{\theta}_3 + b_3\dot{\theta}_3 = T_0 - T_{\text{L}} + f_3 \end{cases} \tag{9}$$

where $f_i(i = 1, 2, 3)$ is model uncertainty.

Here d_1 includes $T_{\text{ice,sta}}$ and f_1, and control law u_1 of the sliding mode controller is equivalent to T_{c}, which are

TABLE 1. Rules of the mode switching.

Number	Mode switching phase	Switching rules	Target state	ICE state	EM state	Clutch state
1	ICE starting phase	$0 < \dot{\theta}_1 < \dot{\theta}_{\text{ice,idle}} \& T_c > T_{\text{ice,sta}}$	$\dot{\theta}_1 = \dot{\theta}_{\text{ice,idle}}$	starting	Electric driving	slipping
2	speed synchronization phase	$\dot{\theta}_{\text{ice,idle}} < \dot{\theta}_1 < \dot{\theta}_2 \& 0 < T < T_{\text{ice,min}}$	$\dot{\theta}_1 = \dot{\theta}_2$	working	Electric driving	slipping
3	torque redistribution phase	$\dot{\theta}_1 = \dot{\theta}_2 \& T_{\text{req}} > T_{\text{ice,max}}$ $\& T_{\text{ice}} \neq T_{\text{ice,req}}$	$T_{\text{ice}} + T_{\text{em}} = T_{\text{req}}$ $\& T_{\text{ice}} = T_{\text{ice,req}}$	working	Electric driving	engagement

Note: $\dot{\theta}_{\text{ice,idle}}$ is the ICE idle angular speed, and $T_{\text{ice,sta}}$ is the ICE starting resisting torque, $T_{\text{ice,min}}$ and $T_{\text{ice,max}}$ are the ICE minimum and maximum working torque,T_{req} is the input torque required for the planetary gears, $T_{\text{ice,req}}$is the ICE requiring torque.

calculated as below.

$$d_1 = -T_{\text{ice,sta}} + f_1 \tag{10}$$
$$u_1 = T_c \tag{11}$$

$\dot{\theta}_{\text{ice,idle}}$ is regarded as target value of this phase, tracking error e_1 and state variable x are calculated as following.

$$e_1 = \theta_1 - \theta_{1,\text{req}} \tag{12}$$
$$x_1 = e_1, \quad x_2 = \dot{e}_1 = \dot{\theta}_1 - \dot{\theta}_{1,\text{req}} \tag{13}$$

where $\dot{\theta}_{1,\text{req}}$ is requiring angular speed of this phase.

Assuming $k_1 = -b_1\dot{\theta}_{1,\text{req}}/J_1$, state equation is as below.

$$\begin{bmatrix} \dot{x_1} \\ \dot{x_2} \end{bmatrix} = \begin{bmatrix} 0 & 1 \\ 0 & -\frac{b_1}{J_1} \end{bmatrix} \begin{bmatrix} x_1 \\ x_2 \end{bmatrix} + \begin{bmatrix} 0 \\ \frac{1}{J_1} \end{bmatrix} u_1 + \begin{bmatrix} 0 \\ \frac{1}{J_1} \end{bmatrix} d_1 + \begin{bmatrix} 0 \\ k_1 \end{bmatrix} \tag{14}$$

Switching function s_1 of the sliding mode controller is supposed to compute as follows.

$$s_1 = c_1 e_1 + \dot{e}_1 \tag{15}$$

where c_1 is positive constant.

Both sides of Eq. (15) are differentiated by time and Eq. (14) is substituted in Eq. (15). The result is this.

$$\dot{s}_1 = c_1\dot{e}_1 - \frac{b_1}{J_1}x_2 + \frac{1}{J_1}u_{s1} + \frac{1}{J_1}d_1 + k_1 \tag{16}$$

where u_{s1} is the sliding mode controller.

The saturation function substitutes for sign function to reduce system dithering, which uses exponential approach law.

$$\dot{s}_1 = -\varepsilon_1 sat(s_1) - \sigma_1 s_1 \tag{17}$$

where $sat(s_1)$ is the saturation function.

$sat(s_1)$is counted as below.

$$sat(s_1) = \begin{cases} s_1/|s_1|, & |s_1| \geq \phi \\ s_1/\phi, & |s_1| < \phi,\ \phi > 0,\ \alpha_1 > 0,\ \beta_1 > 0 \end{cases} \tag{18}$$

From Eqs. (16 - 18), the sliding mode controller is obtained.

$$u_{s1} = b_1 x_2 - d_1 - J_1[c_1\dot{e}_1 + \varepsilon_1 sat(s_1) + \sigma_1 s_1 + k_1] \tag{19}$$

If the sliding mode controller is adopted alone, the system dithering is enhanced for the gain is too large. Therefore, the sliding mode control should be combined with interference compensation to lessen the gain. In consideration of the error between actual model and nominal model, d_1 is rewrote as this.

$$d_1' = d_1 + (b_1^n - b_1)x_2 + (J_1^n - J_1)\dot{x}_2 + (\frac{J_1}{J_1^n} - 1)u_1 \tag{20}$$

where superscript n is nominal model.

From Eq. (19), d_1' includes d_1 and the error of system model, and then the state equation is rewrote as below.

$$\begin{bmatrix} \dot{d_1'} \\ \dot{x}_2 \end{bmatrix} = \begin{bmatrix} 0 & 0 \\ \frac{1}{J_1} & -\frac{b_1}{J_1} \end{bmatrix} \begin{bmatrix} d_1' \\ x_2 \end{bmatrix} + \begin{bmatrix} 0 \\ \frac{1}{J_1} \end{bmatrix} u_1 + \begin{bmatrix} 0 \\ k_1 \end{bmatrix} \tag{21}$$

The disturbance observer is designed as following to estimate d_1'.

$$\begin{bmatrix} \dot{\hat{d}}_1' \\ \dot{\hat{x}}_2 \end{bmatrix} = \begin{bmatrix} 0 & 0 \\ \frac{1}{J_1} & -\frac{b_1}{J_1} \end{bmatrix} \begin{bmatrix} \hat{d}_1' \\ \hat{x}_2 \end{bmatrix} + \begin{bmatrix} 0 \\ \frac{1}{J_1} \end{bmatrix} u_1 + \begin{bmatrix} 0 \\ k_1 \end{bmatrix} + \begin{bmatrix} K_1 \\ K_2 \end{bmatrix} [x_2 - \hat{x}_2] \tag{22}$$

where $\hat{d}_1'$ and $\hat{x}_2$ are the estimated values of d_1' and x_2, K_1 and K_2 are gains through pole assignment.

The sliding mode controller based on interference compensation is devised as this.

$$u_1 = u_{s1} + \hat{d}_1' \tag{23}$$

In a word, the sliding mode controller in ICE starting phase is this.

$$u_1 = b_1 x_2 - d_1 - J_1[c_1\dot{e}_1 + \varepsilon_1 sat(s_1) + \sigma_1 s_1 + k_1] + \hat{d}_1' \tag{24}$$

Stabilization proof of the sliding mode controller is shown as below.

Proof: Constructed Lyapunov function is this.

$$V = V_1 + V_2 = \frac{1}{2}s_1^2 + \frac{1}{2J_1K_1}\tilde{d}_1'^2 + \frac{1}{2}\tilde{x}_2^2 \tag{25}$$

where

$$\begin{cases} V_1 = \frac{1}{2}s_1^2 \\ V_2 = \frac{1}{2J_1K_1}\tilde{d}_1'^2 + \frac{1}{2}\tilde{x}_2^2 \\ \tilde{d}_1' = d_1' - \hat{d}_1' \\ \tilde{x}_2' = x_2 - \hat{x}_2 \end{cases} \tag{26}$$

Both sides of Eq. (25) are differentiated by time and Eq. (17) is substituted in Eq. (25). The result is this.

$$\dot{V}_1 = s_1\dot{s}_1 = -\alpha_1|s_1| - \beta_1 s_1^2 \leq 0 \tag{27}$$

$$\dot{V}_2 = \frac{1}{J_1K_1}\tilde{d}_1'\dot{\tilde{d}}_1' + \tilde{x}_2\dot{\tilde{x}}_2 = \frac{1}{J_1K_1}\tilde{d}_1'(\dot{d}_1' - \dot{\hat{d}}_1') + \tilde{x}_2(\dot{x}_2 - \dot{\hat{x}}_2) \tag{28}$$

$\dot{x}_2$, $\dot{\hat{d}}_1'$ and $\dot{\hat{x}}_2$ in Eqs. (21-22), and $\dot{d}_1' = 0$ are substituted in Eq. (28). The result is this.

$$\dot{V}_2 = -\frac{1}{J_1}\tilde{d}_1'\tilde{x}_2 + \tilde{x}_2[\frac{1}{J_1}\tilde{d}_1' - \frac{b_1}{J_1}\tilde{x}_2 - K_2\tilde{x}_2] = (-\frac{b_1}{J_1} - K_2)\tilde{x}_2^2 \tag{29}$$

When $K_1 > 0$ and $K_2 > -b_1/J_1$, $\dot{V}_2 \leq 0$. Furthermore, $\dot{V}_1 \leq 0$ from Eq. (27). V is nonincreasing function, that is, s_1 and $\tilde{x_2}$ are bounded, so $\dot{e_1}$ and tracking error e_1 are bounded.

These ensure that s_1 and e_1 are asymptotically stable. In a word, it is testified that the control law designed could ensure system stability, and ICE reaching idling speed and finishing starting.

2) SPEED SYNCHRONIZATION PHASE

In this phase, ICE angular speed goes through from $\dot{\theta}_{\text{ice,idle}}$ to synchronous speed in the aid of EM. The clutch is still in slipping state, that is $\dot{\theta}_1$, isn't equal to $\dot{\theta}_2$. Here HEV dynamics equations are expressed as follows.

$$\begin{cases} J_1\ddot{\theta}_1 + b_1\dot{\theta}_1 = T_{\text{ice}} + T_{\text{c}} + f_1 \\ J_2\ddot{\theta}_2 + b_2\dot{\theta}_2 = \dfrac{T_{\text{em}}}{i_{\text{g}}} - \dfrac{T_0}{i_{\text{g}} i_0} - T_{\text{c}} + f_2 \\ J_3\ddot{\theta}_3 + b_3\dot{\theta}_3 = T_0 - T_{\text{L}} + f_3 \end{cases} \tag{30}$$

Owning to delay of ICE dynamic response, there is deviation $T_{\text{ice,err}}$ between its actual output torque T_{ice} and torque required $T_{\text{ice,req}}$.

$$T_{\text{ice,err}} = T_{\text{ice,req}} - T_{\text{ice}} \tag{31}$$

Here, d_2 consists of ICE speed error and model uncertainty. The dynamics equations at driven plate side of clutch are expressed as follows.

$$J_1\ddot{\theta}_1 + b_1\dot{\theta}_1 = T_{\text{ice,req}} + u_2 + d_2 \tag{32}$$

where

$$\begin{cases} d_2 = -T_{\text{ice,err}} + f_1 \\ u_2 = T_{\text{c}} \end{cases} \tag{33}$$

EM speed is set as target value of this phase.

$$\dot{\theta}'_{2,\text{req}} = \dot{\theta}_2 \tag{34}$$

where $\dot{\theta}'_{2,\text{req}}$ is speed required of this phase.

So, tracking error e_2 and state value x are these respectively.

$$e_2 = \theta_1 - \theta'_{2,\text{req}} \tag{35}$$

$$x_1 = e_2, \quad x_2 = \dot{e}_2 = \dot{\theta}_1 - \dot{\theta}'_{2,\text{req}} \tag{36}$$

Switching function s_2 of the sliding mode controller is supposed to compute as following.

$$s_2 = c_2 e_2 + \dot{e}_2 \tag{37}$$

where c_2 is positive constant.

Like d'_1, d'_2 also includes d_2 and the error of system model, and its equation is as below.

$$d'_2 = d_2 + (b_1^n - b_1)x_2 + (J_1^n - J_1)\dot{x}_2 + (\frac{J_1}{J_1^n} - 1)u_2 \tag{38}$$

Supposing $k_2 = -\ddot{\theta}'_{2,\text{req}} - b_1\dot{\theta}'_{2,\text{req}}/J_1 + T_{\text{ice,req}}/J_1$, disturbance observer is designed as follows.

$$\begin{bmatrix} \dot{\hat{d}}'_2 \\ \dot{\hat{x}}_2 \end{bmatrix} = \begin{bmatrix} 0 & 0 \\ \dfrac{1}{J_1} & -\dfrac{b_1}{J_1} \end{bmatrix} \begin{bmatrix} \hat{d}'_2 \\ \hat{x}_2 \end{bmatrix} + \begin{bmatrix} 0 \\ \dfrac{1}{J_1} \end{bmatrix} u_2 + \begin{bmatrix} 0 \\ k_2 \end{bmatrix} + \begin{bmatrix} K_3 \\ K_4 \end{bmatrix} [x_2 - \hat{x}_2] \tag{39}$$

where $\hat{d}'_2$ is the estimated value of d'_2, K_3 and K_4 are gains through pole assignment.

In a word, the sliding mode controller in speed synchronization phase is this.

$$u_2 = b_1 x_2 - d_2 - J_1[c_2\dot{e}_1 + \varepsilon_2 sat(s_2) + \sigma_2 s_2 + k_2] + \hat{d}'_2 \tag{40}$$

where $\varepsilon_2 > 0, \sigma_2 > 0,$.

Stabilization proof of the sliding mode controller in this phase is similar to that in ICE starting phase and will not be described here.

3) TORQUE REDISTRIBUTION PHASE

In this phase, the clutch is in total engagement and ICE angular speed has synchronized with EM. According to HEV torque required, EM torque need to compensate for error of ICE torque, that is, target torque of these two power sources need redistribution to ensure wheel torque unchanged before and after switching. Here, the clutch is in total engagement, that is, $\dot{\theta}_1$ is equal to $\dot{\theta}_2$. HEV dynamics equations are expressed as follows.

$$\begin{cases} (J_1 + J_2)\ddot{\theta}_2 + (b_1 + b_2)\dot{\theta}_2 = T_{ice} + T_{\text{em}} - T_0/i_g i_0 + f_1 + f_2 \\ J_3\ddot{\theta}_3 + b_3\dot{\theta}_3 = T_0 - T_1 + f_3 \end{cases} \tag{41}$$

From Eq. (41), the result is this.

$$(J_1 + J_2)\ddot{\theta}_2 + J_3\ddot{\theta}_3 + (b_1 + b_2)\dot{\theta}_2 + b_3\dot{\theta}_3 = T_{\text{ice}} + T_{\text{em}} + (1 - 1/i_{\text{g}} i_0)T_0 - T_1 + f_1 + f_2 + f_3 \tag{42}$$

Here, d_3 includes the error of ICE torque system model uncertainty and $T_{\text{em,req}}$ is regarded as control law u_3.

$$d_3 = -T_{\text{ice,err}} + f_1 + f_2 + f_3 \tag{43}$$

$$u_3 = T_{\text{em,req}} \tag{44}$$

According to Eqs. (42-43), Eq. (41) could be rewrote as below.

$$(J_1 + J_2)\ddot{\theta}_2 + J_3\ddot{\theta}_3 + (b_1 + b_2)\dot{\theta}_2 + b_3\dot{\theta}_3 = T_{\text{ice,req}} + u_3 + (1 - 1/i_{\text{g}} i_0)T_0 - T_1 + d_3 \tag{45}$$

The HEV reference models in this phase are as follows to achieve smooth switching from pure electric driving mode to hybrid driving mode.

$$\begin{cases} (J_1 + J_2)\ddot{\theta}_{2,\text{ref}} + (b_1 + b_2)\dot{\theta}_{2,\text{ref}} = T_{\text{ice,ref}} \\ \qquad + T_{\text{em,ref}} - T_{0,\text{ref}}/i_{\text{g}} i_0 + f_1 + f_2 \\ J_3\ddot{\theta}_{3,\text{ref}} + b_3\dot{\theta}_{3,\text{ref}} = T_{0,\text{ref}} - T_1 + f_3 \end{cases} \tag{46}$$

where subscript ref is reference value of the parameters.

Wheel speed $\dot{\theta}_{3,\text{ref}}$ in HEV reference models is set as target value of this phase.

$$\dot{\theta}_{3,\text{req}} = \dot{\theta}_{3,\text{ref}} \tag{47}$$

where $\dot{\theta}_{3,\text{req}}$ is speed required of this phase.

So, tracking error e_3 and state value x are these respectively.

$$e_3 = \theta_3 - \theta_{3,\text{req}} \tag{48}$$

$$x_1 = e_3, x_2 = \dot{e}_3 \tag{49}$$

Switching function s_3 of the sliding mode controller is supposed to compute as following.

$$s_3 = c_3 e_3 + \dot{e}_3 \tag{50}$$

where c_3 is positive constant.

Like d_1', d_3' also includes d_3 and the error of system model, and its equation is as below.

$$d_3' = d_3 + (b_3^n - b_3)x_2 + (J_3^n - J_3)\dot{x}_2 + (J_3/J_3^n - 1)u_3 \tag{51}$$

Supposing, $k_3 = -[J_1 + J_2']\ddot{\theta}_2 + (b_1 + b_2)\dot{\theta}_2 + b_3\dot{\theta}_{3,\text{req}} - (T_{\text{ice,req}} + (1 - 1/i_g i_0)T_0 - T_1)]/J_3$, disturbance observer is designed as follows.

$$\begin{bmatrix} \dot{\hat{d}}_3' \\ \dot{\hat{x}}_2 \end{bmatrix} = \begin{bmatrix} 0 & 0 \\ \dfrac{1}{J_3} & -\dfrac{b_3}{J_3} \end{bmatrix} \begin{bmatrix} \hat{d}_3' \\ \hat{x}_2 \end{bmatrix} + \begin{bmatrix} 0 \\ \dfrac{1}{J_3} \end{bmatrix} u_3 + \begin{bmatrix} 0 \\ k_3 \end{bmatrix} + \begin{bmatrix} K_5 \\ K_6 \end{bmatrix} [x_2 - \hat{x}_2] \tag{52}$$

where $\hat{d}_3'$ is the estimated value of d_3', K_5 and K_6 are gains through pole assignment.

In a word, the sliding mode controller in torque redistribution phase is this.

$$u_3 = b_3 x_2 - d_3 - J_3[c_3\dot{e}_3 + \varepsilon_3 sat(s_3) + \sigma_3 s_3 + k_3] + \hat{d}_3' \tag{53}$$

where $\varepsilon_3 > 0, \sigma_3 > 0$.

Stabilization proof of the sliding mode controller in this phase is similar to that in ICE starting phase and will not be described here.

V. RESULTS AND DISCUSSION

The evaluation is performed by using both simulation environment and experimental tests.

To show the effectiveness of the proposed sliding mode control method based on disturbance compensation in the dynamic coordinated control, three control strategies (i.e., the online estimation of the ICE speed, MPC, sliding mode control based on disturbance compensation) are proposed for the comparison purpose. They are respectively simplified as Strategy 1, Strategy 2 and Strategy 3.

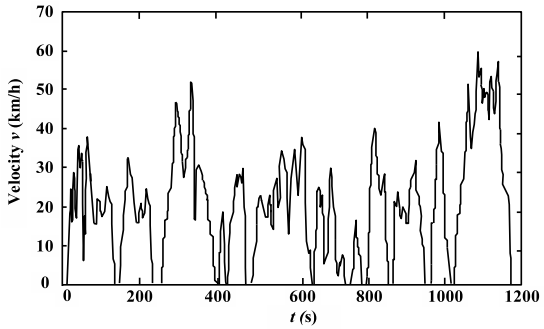

FIGURE 14. Comprehensive driving cycle of local passenger vehicles.

TABLE 2. Numerical values of the vehicle and main parts parameters.

Component	Parameter	Value
Vehicle	air resistance coefficient C_D	0.31
	frontal area A	$2m^2$
	vehicle total mass m	1381kg
	wheel rolling radius r	0.283
	rolling resistance coefficients f_0	1.1×10^{-2}
	rolling resistance coefficients f_1	2.6×10^{-4}
	rolling resistance coefficients f_4	6.5×10^{-4}
ICE	maximum power	51kW(5600r/min)
	maximum torque	90Nm(4600r/min)
	peak efficiency	0.393
EM	voltage	380(v)
	nominal power	45kW
	nominal torque	173Nm
	peak efficiency	0.90
Battery	type	Li-ion
	Nominal voltage of a module	48v
	Nominal capacity of a module	20Ah
	Number of modules	8

A. SIMULATION RESULTS AND ANALYSIS

The effectiveness of the proposed control method is appraised under the real driving cycle shown in Fig. 14 by using the data acquisition system named VBOX3i based on GPS [34]. Numerical values of the vehicle parameters and main parts are listed in Table 2. Values of the dynamics parameters are displayed in Table 3. Using models built in Section III, three control strategies comparative simulation has been accomplished in the Matlab / Simulink / BondHEV environment.

The comparative simulation results are shown in Fig. 15. At the 5.8s, the torque required of HEV begins to increase, the vehicle need switching from pure electric driving mode to hybrid driving mode. Seen from Fig. 15 (a) and (c), EM torques and speed both start to rise. When the clutch friction

TABLE 3. Numerical values of the dynamic parameters.

Parameter	Value	Parameter	Value
Inertia moment of ICE J_{ice}	0.121 kg· m^2	clutch inertia moment of the driven disc J_{cm}	0.018 kg· m^2
Inertia moment of EM J_{em}	0.167kg · m^2	damping coefficient of ICE side b_1	0.017 N· m · s/rad
Inertia moment of Wheel J_w	0.25 kg · m^2	damping coefficient of EM side b_2	0.113 N· m · s/rad
Inertia moment of planetary gears J_g	0.185 kg · m^2	damping coefficient of wheel side b_3	0.054 N· m · s/rad
Inertia moment of driving axle J_0	0.224 kg · m^2	characteristic parameter of planetary gears k	1.45
Clutch inertia moment of the driving disc J_{ce}	0.025 kg· m^2	gear ratio of main reducing gear i_0	3.5

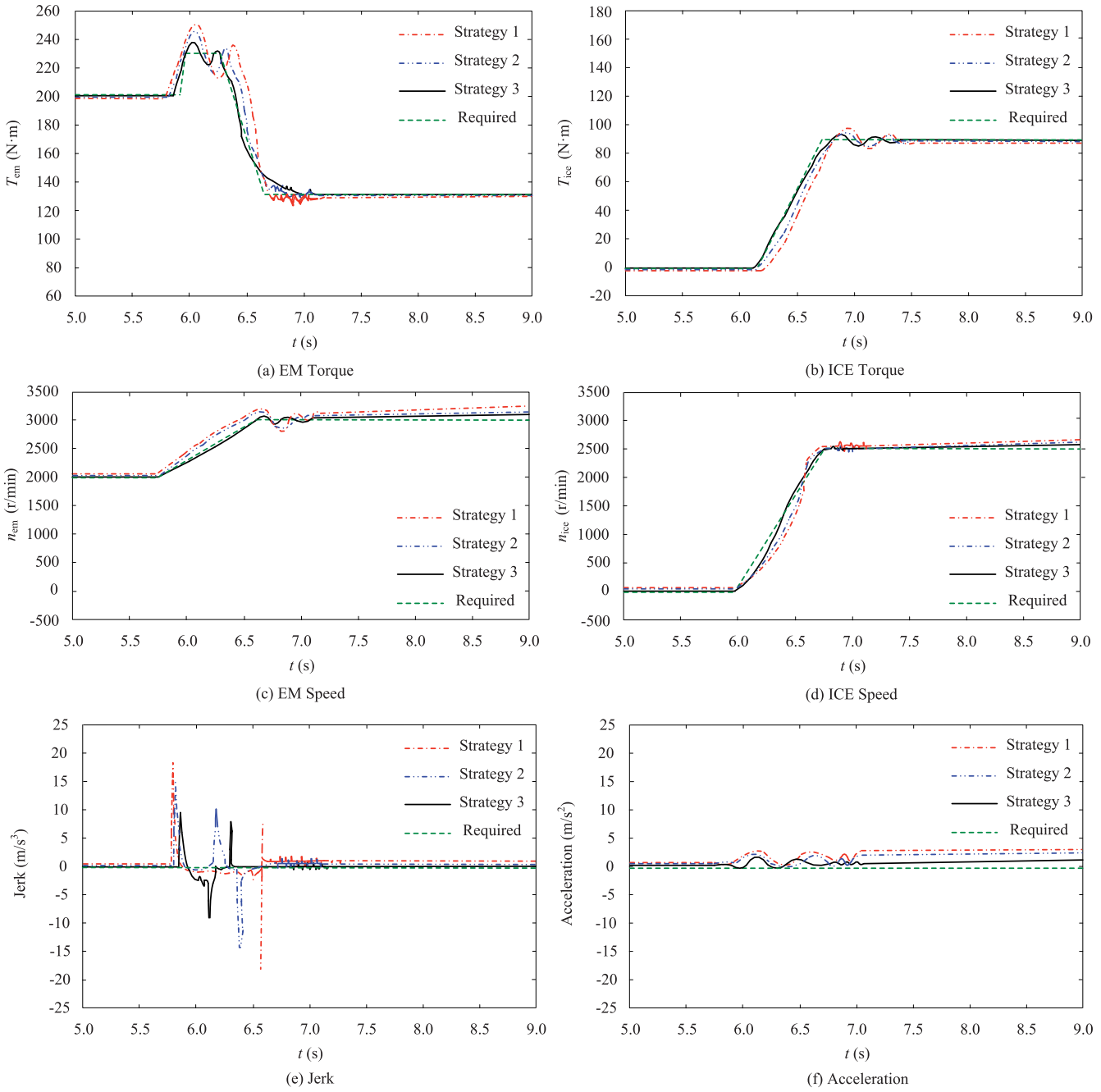

FIGURE 15. The comparative simulation results among three strategies from pure electric driving mode to hybrid driving mode.

torque is larger than ICE resistance torque, ICE begins to start at the 6.0 s, seen from Fig. 15 (b) and (d). With Strategy 3, it takes 0.3 s for ICE from 0 to 800 r/min, then the period from 6.3s to 6.6s belongs to speed synchronization phase. After 6.6s, the clutch is in full engagement and the mode switching enters torque redistribution phase, in which EM torque decreases, and ICE torque increases until their torques follow the target torque entirely. The mode switching is accomplished.

Compared with Strategy 1 and Strategy 2, the variation of EM torque with Strategy 3 is slowest so as to drive ICE starting, whose curve is closest to the curve required. From Fig. 15 (a), the maximum fluctuation of EM torque is 20 N·m, 15 N·m and 10 N·m respectively for Strategy 1, Strategy 2 and Strategy 3. Among three strategies, the change of ICE torque with Strategy 3 is fastest owing to EM driving, whose curve is closest to the curve required. From Fig. 15 (b), the maximum fluctuation of ICE torque is 9 N·m, 6 N·m and 4 N·m respectively for Strategy 1, Strategy 2 and Strategy 3, which are all much smaller than that of EM. The time that ICE takes from 0 to 800 r/min is prolonged to 0.40s and 0.35s by Strategy 1 and Strategy 2 respectively, seen from Fig. 15 (d).

TABLE 4. The comparative simulation results among three strategies during mode switching with ice starting.

Mode Switching	Strategy 1		Strategy 2		Strategy 3	
	Maximum torque fluctuation /(N· m)	Maximum Jerk /(m/s^3)	Maximum torque fluctuation /(N· m)	Maximum Jerk /(m/s^3)	Maximum torque fluctuation /(N·m)	Maximum Jerk /(m/s^3)
pure electric driving → ICE driving	17.3	15.4	13.7	12.4	8.1	7.2
pure electric driving → charging in driving	23.2	21.5	18.2	16.5	11.7	11.0
pure electric driving → hybrid driving	20.0	18.5	15.0	15.0	10.0	9.5

1. ICE and its controller; 2. Tested vehicle; 3. Dynamometer; 4. Inverter system; 5. Vehicle controller; 6. EM and its controller; 7. Battery and its controller; 8. Centralized control system.

FIGURE 16. HEV experiment platform.

In Fig. 15 (e), the maximum jerk is up to 18.5 m/s^3 and 15 m/s^3 for Strategy 1, Strategy 2 respectively, which are both larger than 10 m/s^3 (German index limit value), whereas that for Strategy 3 is as low as 9.5 m/s^3 and smaller than German index limit value. From Fig. 15 (f), the maximum accelerations of three strategies aren't all large and are in an acceptable range.

In the same way, other mode switching with ICE starting is also simulated. Maximum torque fluctuation and maximum Jerk are regarded as evaluating indicators, and the comparative simulation results among three strategies during mode switching with ICE starting are shown in Table 4.

From Table 4, the proposed sliding mode control method based on disturbance compensation improves the ride comfort and reduces the jerk during mode switching. Although these simulations are accomplished under the given driving cycle, and mode switching could happen at arbitrary velocity and torque required, switching rules and general principles of torque coordinated control are the same. Therefore, these simulation results could testify to the rationality of the control method designed.

B. EXPERIMENTAL RESULTS AND ANALYSIS

The characteristics of simulations are easy to be implemented and have lower cost, but they can't reflect situations comprehensively and actually, and many unpredictable problems in real applications are still potential factors. Thus, the experiment platform is established to confirm simulation results.

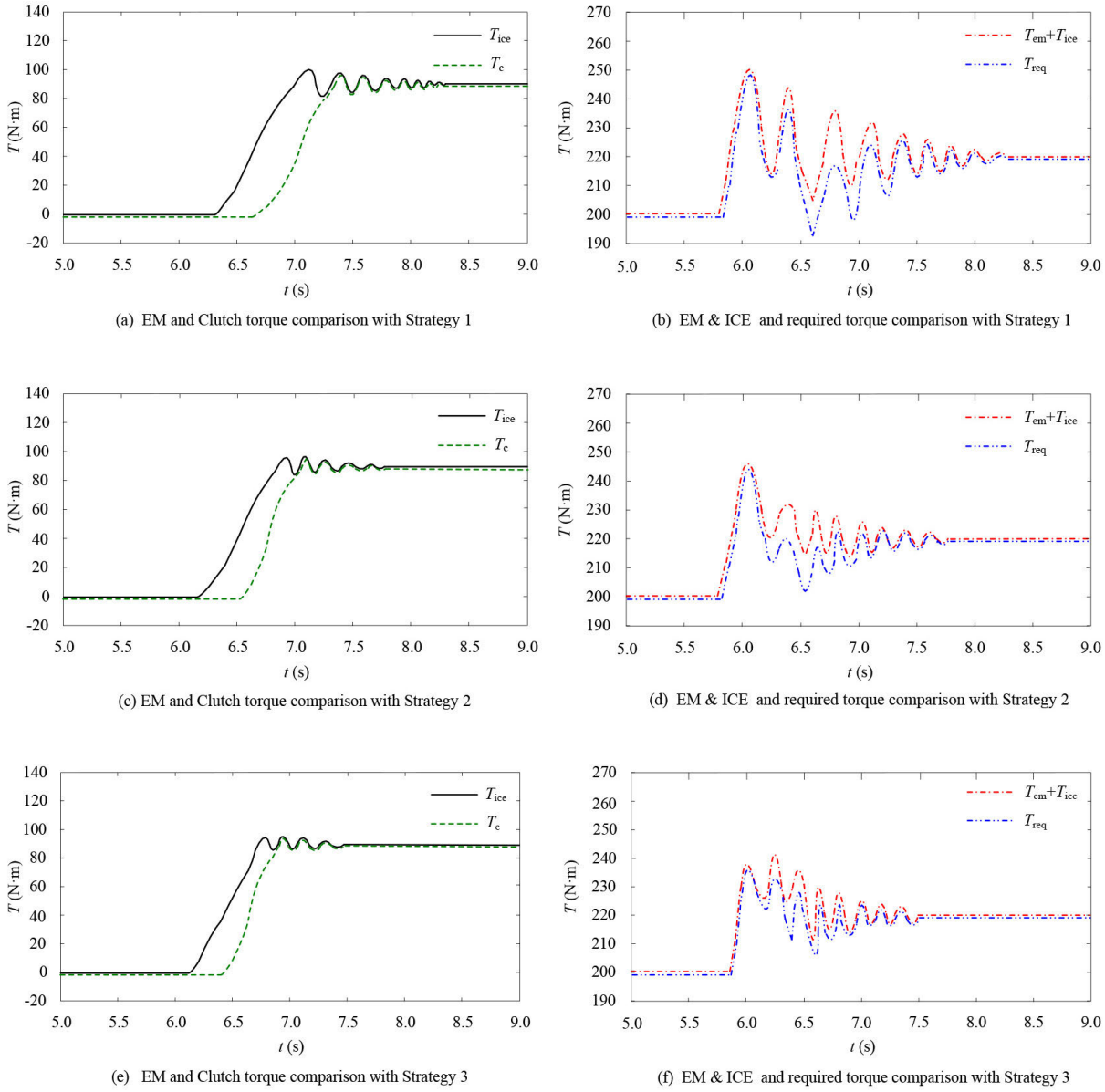

(a) EM and Clutch torque comparison with Strategy 1
(b) EM & ICE and required torque comparison with Strategy 1
(c) EM and Clutch torque comparison with Strategy 2
(d) EM & ICE and required torque comparison with Strategy 2
(e) EM and Clutch torque comparison with Strategy 3
(f) EM & ICE and required torque comparison with Strategy 3

FIGURE 17. The comparative experimental results among three strategies from pure electric driving mode to hybrid driving mode.

Fig. 16 shows the structure of the HEV experiment platform which is composed of the HEV, dynamometer, ICE and EM and battery and their corresponding controller, inverter and centralized control system. Under the comprehensive driving cycle of local passenger vehicles shown in Fig. 14, the experimental results are shown in Fig.17 from pure electric driving mode to hybrid driving mode.

T_c is compared with T_{ice} in Fig. 17 (a), (c) and (e) among three strategies. In the ICE starting phase, T_c is equal to zero, but the duration is different, in which the ICE starting time with Strategy 3 is shortest. In the speed synchronization phase, T_c is increased gradually during the clutch engagement, but the rate of change with Strategy 3 is fastest. In the torque redistribution phase, T_c is equal to T_{ice}, then the power can be transmitted to the planetary gears to drive the wheel. From Fig. 17 (a), (c) and (e), the fluctuation of T_{ice} is also different among three strategies. The time of T_{ice} fluctuation with Strategy 1 is longest and its range is widest. By contrast, its time is shortest and its range is narrowest with Strategy 3. For details, see Table 5, Table 6 and Table 7.

T_{req} is compared with T_{ice} plus T_{em} in Fig. 17 (b), (d) and (f) among three strategies. In the ICE starting phase, T_{req} is equal to T_{em}, and T_{req} is less than T_{ice} plus T_{em} in the speed synchronization phase, and T_{req} is equal to T_{ice} plus T_{em} in the torque redistribution phase. From Fig. 17 (b), (d) and (f), the fluctuation of T_{ice} plus T_{em} is also different among three strategies. Compared with Strategy 1 and Strategy 2, the variations of T_{ice} plus T_{em} on the horizontal axis and vertical axis are narrower with Strategy 3. Moreover, T_{req} follows T_{ice} plus T_{em} seen from Fig. 17 (b), (d) and (f). The deviation from

TABLE 5. The experimental results with Strategy 1 during mode switching with ICE starting.

Mode Switching	Maximum torque fluctuation /(N·m)	Maximum Jerk (m/s^3)	Maximum acceleration (m/s^2)	Mode Switching time (s)
pure electric driving → ICE driving	20.7	17.8	2.3	1.7
pure electric driving → charging in drivin g	27.0	24.6	3.2	2.6
pure electric driving → hybrid driving	23.5	21.0	2.9	2.3

TABLE 6. The experimental results with Strategy 2 during mode switching with ICE starting.

Mode Switching	Maximum torque fluctuation /(N·m)	Maximum Jerk (m/s^3)	Maximum acceleration (m/s^2)	Mode Switching time (s)
pure electric driving → ICE driving	16.5	13.8	1.9	1.5
pure electric driving → charging in driving	22.0	19.7	2.9	2.3
pure electric driving → hybrid driving	18.6	16.6	2.5	1.8

TABLE 7. The experimental results with Strategy 3 during mode switching with ICE starting.

Mode Switching	Maximum torque fluctuation /(N·m)	Maximum Jerk (m/s^3)	Maximum acceleration (m/s^2)	Mode Switching time (s)
pure electric driving → ICE driving	9.7	7.6	1.3	1.1
pure electric driving → charging in driving	14.5	12.6	2.3	1.8
pure electric driving → hybrid driving	11.7	10.0	1.9	1.5

T_{ice} plus T_{em} with Strategy 3 is obviously less than the other strategies in the speed synchronization phase.

In a word, the ICE and EM power could be transmitted smoothly by using the proposed strategy. The reason is that Strategy 1 and Strategy 2 have poor real-time, whereas the ICE speed and torque with Strategy 3 have quick response with the aid of the EM.

In the same way, other mode switching with ICE starting is also tested. The maximum torque fluctuation, maximum jerk, maximum acceleration and mode switching time are regarded as evaluating indicators, and the comparative experimental results among three strategies during mode switching with ICE starting are listed in Table 5, Table 6 and Table 7 respectively.

Compared with Strategy 1, the maximum torque fluctuation, maximum jerk, maximum acceleration and mode switching time have a decrease of 50.2%, 52.4%, 34.5% and 34.8% respectively with Strategy 3 during mode switching from the pure electric driving to hybrid driving. The four evaluating indicators are reduced by 37.1%, 39.8%, 24.0%and 16.7% respectively relative to Strategy 2. In the same way, during the other mode switching, the values of the four indicators for Strategy 3 are also less than that for Strategy 1 and Strategy 2. Furthermore, these experimental results are consistent with the simulation results. The reason is that the torque disturbance is well compensated for in both clutch slipping and engaged stages by the proposed control strategy. Thus, the vehicle jerk during the mode transition is greatly reduced.

Overall, the results obtained from the HEV experiment platform further verify the performances of the control strategy developed.

VI. CONCLUSION

On the basis of the steady-state and transient models of parts and working modes, a dynamic coordinated control has been developed for an HEV during mode switching with ICE starting. A sliding mode control method based on disturbance compensation is put forward to accomplish torque coordination during mode switching to cope with the system uncontinuity and strong nonlinearity. The switching process from pure electric driving to hybrid driving is divided into three phases that include ICE starting, speed synchronization and torque redistribution in the light of the state of the clutch and ICE and control target. The according disturbance observer and sliding mode controller are designed for each phase and these controllers stabilization is also proved.

The proposed control strategy has been validated by not only computer simulations but also experimental tests by using real vehicle compared with other two control strategies under the comprehensive driving cycle of local passenger vehicles. Four evaluating indicators are put to use including the maximum torque fluctuation, maximum jerk, maximum acceleration and mode switching time to evaluate the ride comfort comprehensively. The results indicate that four evaluating indicators all have a certain decrease and the variation curves of the EM and ICE torque are closest to the curve

required with the control strategy designed during each mode switching with ICE starting.

Thus, the proposed dynamic coordination control strategy has the great potential to decrease HEV jerk and the fluctuations of driving wheel torque, and improve riding comfort and system robustness. This control strategy helps to complete the control theory of the hybrid electric system and promotes the application of such system.

It is interesting to study mode switching between the driving mode and the braking mode in the future research.

REFERENCES

[1] C. C. Chan, "Outlook of electric, hybrid and fuel cell vehicles," *J. Automot. Saf. Energy*, vol. 23, no. 6, pp. 507–516, 2011.
[2] M. F. M. Sabri, K. A. Danapalasingam, and M. F. Rahmat, "A review on hybrid electric vehicles architecture and energy management strategies," *Renew. Sustain. Energy Rev.*, vol. 53, pp. 1433–1442, Jan. 2016.
[3] A. A. Malikopoulos, "Supervisory power management control algorithms for hybrid electric vehicles: A survey," *IEEE Trans. Intell. Transp. Syst.*, vol. 15, no. 5, pp. 1869–1885, Oct. 2014.
[4] J. Wang, Q. N. Wang, and P. Y. Wang, "Mode transition dynamic control for dual-motor hybrid driving system," Warrendale, PA, USA, SAE Tech. Paper 2013-01-2487, 2013.
[5] F. Zhu, L. Chen, C. Yin, and J. Shu, "Dynamic modelling and systematic control during the mode transition for a multi-mode hybrid electric vehicle," *Proc. Inst. Mech. Eng., D, J. Automobile Eng.*, vol. 227, no. 7, pp. 1007–1023, Jul. 2013.
[6] Y. Su, M. Hu, L. Su, D. Qin, T. Zhang, and C. Fu, "Dynamic coordinated control during mode transition process for a compound power-split hybrid electric vehicle," *Mech. Syst. Signal Process.*, vol. 107, pp. 221–240, Jul. 2018.
[7] L. Wang, "Mode transition control for series-parallel hybrid electric bus using fuzzy adaptive sliding mode approach," *J. Mech. Eng.*, vol. 48, no. 14, pp. 119–127, 2012.
[8] L. Chen, G. Xi, and J. Sun, "Torque coordination control during mode transition for a series-parallel hybrid electric vehicle," *IEEE Trans. Veh. Technol.*, vol. 61, no. 7, pp. 2936–2949, Sep. 2012.
[9] Z. Zhi, X. Dai, C. Wang, T. Zhang, and X. Yuan, "Coordinated control of driving mode switching of compound power-split hybrid electric car," *Automotive Eng.*, vol. 37, no. 3, pp. 260–265, 2015.
[10] C. Wang, Z. Zhao, T. Zhang, and M. Li, "Mode transition coordinated control for a compound power-split hybrid car," *Mech. Syst. Signal Process.*, vol. 87, pp. 192–205, Mar. 2017.
[11] Z. Chen, L. Li, Y. Zhang, C. Yang, J. Song, and X. Jiao, "Research on mode transition control for single-shaft parallel hybrid powertrain," *Sci. Sinica Technol.*, vol. 46, no. 1, pp. 91–100, Jan. 2016.
[12] S. Cauet, P. Coirault, and M. Njeh, "Diesel engine torque ripple reduction through LPV control in hybrid electric vehicle powertrain: Experimental results," *Control Eng. Pract.*, vol. 21, no. 12, pp. 1830–1840, Dec. 2013.
[13] R. I. Davis and R. D. Lorenz, "Engine torque ripple cancellation with an integrated starter alternator in a hybrid electric vehicle: Implementation and control," *IEEE Trans. Ind. Appl.*, vol. 39, no. 6, pp. 1765–1774, Nov. 2003.
[14] H. Borhan, A. Vahidi, A. M. Phillips, M. L. Kuang, I. V. Kolmanovsky, and S. Di Cairano, "MPC-based energy management of a power-split hybrid electric vehicle," *IEEE Trans. Control Syst. Technol.*, vol. 20, no. 3, pp. 593–603, May 2012.
[15] O. Dingel, J. Ross, I. Trivic, N. Cavina, and M. Rioli, "Model-based assessment of hybrid powertrain solutions," Warrendale, PA, USA, SAE Tech. Paper 2011-24-0070, 2011.
[16] Y. Mi, Y. Fu, D. Li, C. Wang, P. C. Loh, and P. Wang, "The sliding mode load frequency control for hybrid power system based on disturbance observer," *Int. J. Elect. Power Energy Syst.*, vol. 74, pp. 446–452, Jan. 2016.
[17] Y.-S. Lu and C.-W. Chiu, "A stability-guaranteed integral sliding disturbance observer for systems suffering from disturbances with bounded first time derivatives," *Int. J. Control, Autom. Syst.*, vol. 9, no. 2, pp. 402–409, Apr. 2011.
[18] T. Yi, "Study on the coordinated control issue in parallel hybrid electric system," (in Chinese), Ph.D. dissertation, Dept. Eng., Tsinghua Univ., Beijing, China, 2004.
[19] J. Q. Li, M. G. Ouyang, and M. Zhou, "On board measurement and analysis of the momentary speed of automotive engines," *Automobile Eng.*, vol. 24, no. 1, pp. 41–45, and 67, 2002.
[20] Y. B. Yang, H. M. Chen, and G. D. Zhang, "Estimation of engine torque for parallel hybrid electric vehicle," *Automobile Eng.*, vol. 30, no. 2, pp. 117–120, 2008.
[21] K. Koprubasi, E. R. Westervelt, and G. Rizzoni, "Toward the systematic design of controllers for smooth hybrid electric vehicle mode changes," in *Proc. Amer. Control Conf.*, New York, NY, USA, Jul. 2007, pp. 2985–2990.
[22] Z. Zhao, "Mode transition control for four wheel drive hybrid electric car," *J. Mech. Eng.*, vol. 47, no. 4, pp. 100–109, 2011.
[23] H. Kim, J. Kim, and H. Lee, "Mode transition control using disturbance compensation for a parallel hybrid electric vehicle," *Proc. Inst. Mech. Eng., D, J. Automobile Eng.*, vol. 225, no. 2, pp. 150–166, Feb. 2011.
[24] S. Kim, J. Park, and J. Hong, "Transient control strategy of hybrid electric vehicle during mode change," Warrendale, PA, USA, SAE Tech. Paper 2009-01-0228, 2009.
[25] H. Wang, P. X. Liu, and B. Niu, "Robust fuzzy adaptive tracking control for nonaffine stochastic nonlinear switching systems," *IEEE Trans. Cybern.*, vol. 47, no. 9, pp. 2568–2578, Aug. 2017.
[26] M. Gokasan, S. Bogosyan, and D. J. Goering, "Sliding mode based power-train control for efficiency improvement in series hybrid-electric vehicles," *IEEE Trans. Power Electron.*, vol. 21, no. 3, pp. 779–790, May 2006.
[27] A. Gao, X. Deng, Z. Fu, and M. Zhang, "Optimization of ice start-stop based on MPC for an HEV to improve fuel economy," *Trans. Can. Soc. Mech. Eng.*, vol. 41, no. 3, pp. 355–374, Sep. 2017.
[28] F. C. Hsieh, T. W. Chou, and Y. C. Chen, "Development of power management strategy using dynamic programming for BSG mild HEV," Warrendale, PA, USA, SAE Tech. Paper 2014-01-1811, 2014.
[29] C. Vagg, S. Akehurst, C. J. Brace, and L. Ash, "Stochastic dynamic programming in the real-world control of hybrid electric vehicles," *IEEE Trans. Control Syst. Technol.*, vol. 24, no. 3, pp. 853–866, May 2016.
[30] N. Kim, S. W. Cha, and H. Peng, "Optimal equivalent fuel consumption for hybrid electric vehicles," *IEEE Trans. Control Syst. Technol.*, vol. 20, no. 3, pp. 817–825, May 2012.
[31] A. Nasri, A. Hazzab, I. K. Bousserhane, S. Hadjeri, and P. Sicard, "Fuzzy-sliding mode speed control for two wheels electric vehicle drive," *J. Electr. Eng. Technol.*, vol. 4, no. 4, pp. 499–509, Dec. 2009.
[32] H. Zhang, Y. Zhang, and C. Yin, "Hardware-in-the-loop simulation of robust mode transition control for a series-parallel hybrid electric vehicle," *IEEE Trans. Veh. Technol.*, vol. 65, no. 3, pp. 1059–1069, Mar. 2016.
[33] G. Aiyun, "Hybrid electromechanical coupling system and dynamic coordinated control of HEV," (in Chinese), Ph.D. dissertation, Dept. Eng., Northwestern Polytech. Univ., Xi'an, China, 2019.
[34] A. Gao, X. Deng, M. Zhang, and Z. Fu, "Design and validation of real-time optimal control with ECMS to minimize energy consumption for parallel hybrid electric vehicles," *Math. Problems Eng.*, vol. 2017, Jan. 2017, Art. no. 3095347.

AIYUN GAO was born in Xihua, Henan, China, in 1974. She received the B.S. degree in mechanical design and manufacture and the M.S. degree in vehicle engineering from the Henan University of Science and Technology, Luoyang, in 1998 and 2001, respectively, and the Ph.D. degree in mechanical design and theory from Northwestern Polytechnical University, Xi'an, China, in 2019. She has over 18 years of extensive experience in the field of hybrid electric vehicles. Since 2010, she has been an Associate Professor with the School of Vehicle and Transportation Engineering, Henan University of Science and Technology. She has been leading or participated in over ten research projects, and has published more than 60 academic articles which are published in prestigious journals. She is the author of three books and more than 30 inventions. Her research interests include model and simulation of the powertrain for hybrid electric vehicles, the design of control strategy for hybrid electric vehicles, and the optimization and matching of parameters for electric vehicles.

ZHUMU FU was born in Xiantao, Hubei, China, in 1974. He received the B.S. degree in mechanical design and manufacture and the M.S. degree in vehicle engineering from the Henan University of Science and Technology, Luoyang, in 1998 and 2003, respectively, and the Ph.D. degree in control theory and control engineering from Southeast University, Nanjing, China, in 2007. He has over 18 years of extensive experience in the field of hybrid electric vehicles. Since 2015, he has been a Professor with the School of Information Engineering, Henan University of Science and Technology. He has been leading or participated in over 40 research projects, and has published more than 120 academic articles which are published in prestigious journals. He is the author of five books and more than 54 inventions. His research interests include theory and application of complex dynamic systems, energy management for hybrid electric vehicles, and coordinated control and optimization of multimode switching for hybrid electric vehicles.

FAZHAN TAO was born in Weifang, Shandong, China, in 1988. He received the Ph.D. degree in electronic and information engineering from the Tokyo University of Agriculture and Technology, Tokyo, Japan, in 2017. He is currently a Lecturer with the School of Information Engineering, Henan University of Science and Technology. He has been leading or participated in over 10 research projects, and has published more than 20 academic articles which are published in prestigious journals. He is the author of two books and more than ten inventions. His research interests include theory and application of nonlinear control, energy management for hybrid electric vehicles, and control and optimization of mode switching for hybrid electric vehicles.